Supramolecular structure of self-assembled oligomers under confinement

Jarosław Paturej[†#*], Kajetan Koperwas[†], Magdalena Tarnacka[†], Karolina Jurkiewicz[†], Paulina Maksym[$], Joanna Grelska[†], Marian Paluch[†], Kamil Kamiński[†]

† *August Chełkowski Institute of Physics, University of Silesia in Katowice, 75 Pułku Piechoty 1, 41-500 Chorzów, Poland*
# *Leibniz-Institut für Polymerforschung, Dresden e.V., Hohe Str. 6, 01069 Dresden, Germany*
$ *Institute of Materials Engineering, University of Silesia, 75 Pułku Piechoty 1a, 41-500 Chorzow, Poland*
* Corresponding author: (JP) jaroslaw.paturej@us.edu.pl

Supporting Information

EXPERIMENTAL SECTION

Material. Poly(mercaptopropyl)methylsiloxane oligomer (PMMS, 75-150 cSt) was purchased from Gelest and used as received. The studied PMMS is characterized by the molecular weight, M_{nSEC}=2.4 kg/mol, and dispersity, Đ=1.26 (as determined by Viscotek TDA 305 triple detection, THF as eluent)[1]. Poly(methylphenylsiloxane) (PMPS) of molecular weights, M_n = 2530 g/mol and Đ=1.4 was purchased from Polymer Source Inc. [2] The poly(methylmercaptopropyl)-grafted-hexylmethacrylate, PMMS-g-HMA was synthesized according to the following procedure. PMMS (0.25 g, 0.05 mmol), nHMA (0.5 g, 2.94 mmol) and DMPA (0.09 g, 0.36 mmol) were dissolved in THF (2 mL). The solution was purged under nitrogen and purified by one freeze-pump-thaw cycle. Next, the flask was stirred for 160 min under UV irradiation, and then THF was evaporated under vacuum. The polymer was purified by washing many times first in methanol/water mixture and then methanol. The purified sample was dried to a constant mass under reduced pressure. The structure of obtained PMMs-g-HMA was verified by NMR experiments. Note that NMR spectra were recorded on using 500 MHz spectrometer (Bruker) for samples in commercially available DMSO-d_6. The results are presented below.

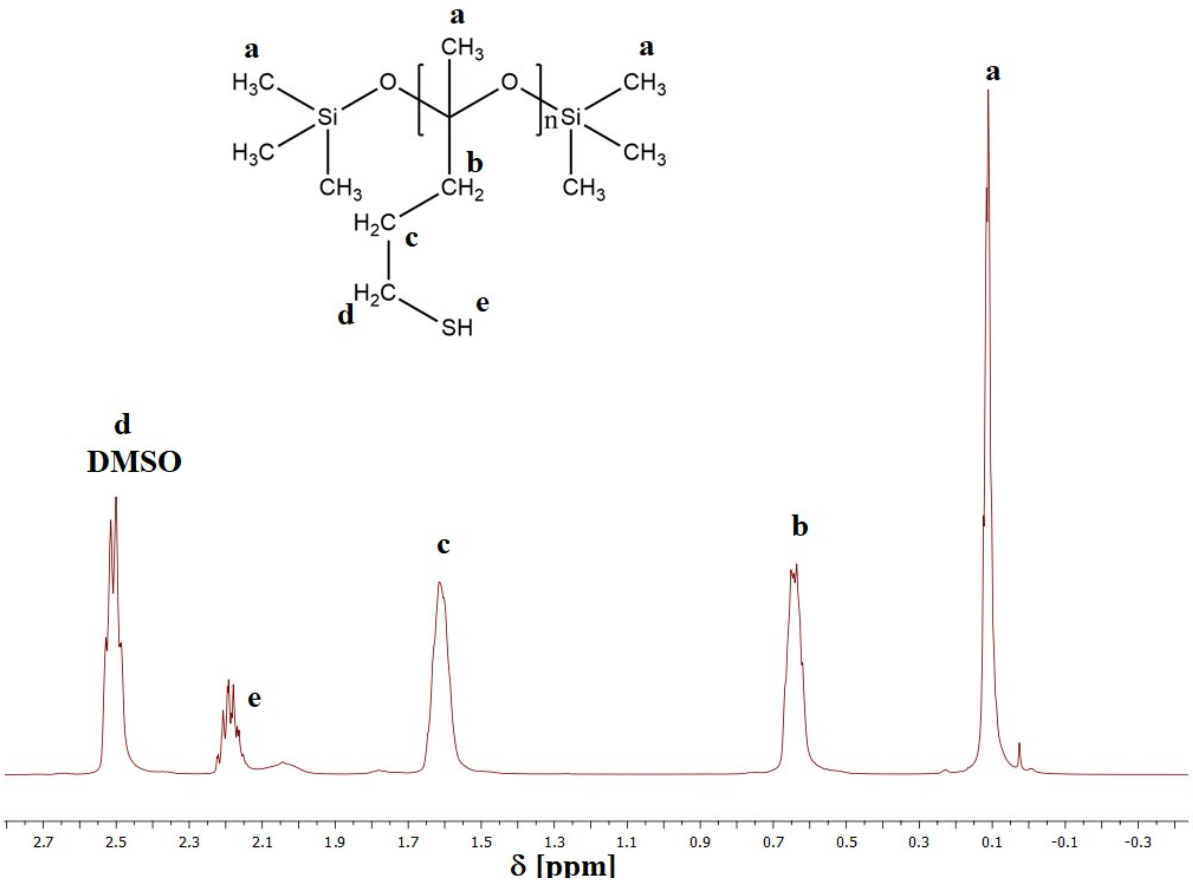

Fig S1. ^{1}H NMR spectrum of commercially available PMMS.

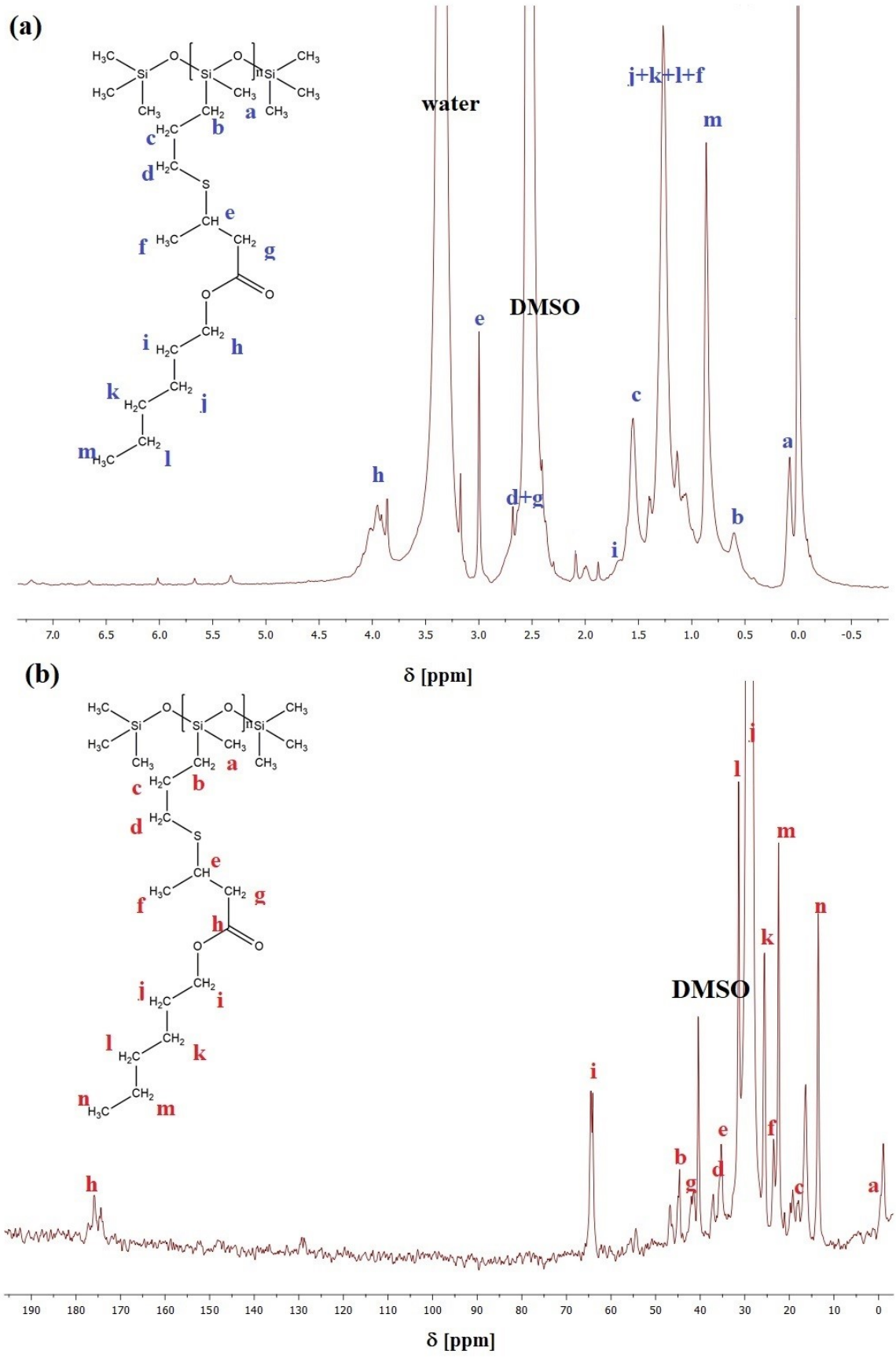

Fig S2. (a) ^{1}H NMR spectrum of PMMS-graft-PHMA, (b) ^{13}C NMR spectrum of PMMS-graft-PHMA

The nanoporous silica membranes were prepared by electrochemical etching of silicon wafers and subsequent thermal oxidation[3,4]. In the experiment, we used silica templates of d = 8nm and d = 4 nm. The pore size distribution of self-made silica templates was confirmed by measuring the nitrogen adsorption/desorption isotherms, see Ref. [5].

Sample preparation/Infiltration procedure. Prior to filling, porous membranes were dried in an oven at T = 423 K under vacuum to remove any volatile impurities from the nanochannels. After cooling, they were placed in PMMS or PMPS. Then, the whole system was maintained at T = 303 K in a vacuum (10^{-2} bar) for t = 24 h to let the compound flow into the nanocavities. After completing the infiltration process, the surface of silica membrane was dried and the excess sample on the porous surface was removed by use of metal blade and paper towel. The complete filling was obtained by weighing the templates before and after each infiltration to constant mass.

X-ray diffraction (XRD). XRD data were collected on a Rigaku Denki D/Max Rapid II diffractometer equipped with a rotating Ag anode, an incident beam graphite (002) monochromator and an image plate in the Debye-Scherrer geometry as a detector. The investigated bulk samples were packed into glass capillaries with a diameter of 1.5 mm and wall thickness of 0.01 mm. The diffraction intensity for the empty capillary was then subtracted. The X-ray beam size at the sample was 0.3 mm. 2D diffraction pattern was azimuthally integrated and converted into one-dimensional function of intensity versus the scattering vector, $q = 4\pi sin\theta/\lambda$, where: 2θ is the scattering angle and λ = 0.5608 Å is the wavelength of the incident X-ray beam. Next, the obtained intensity function was corrected for background, polarization, absorption, incoherent Compton scattering, and normalized to the electron units. After the data correction, the experimental structure factor, $S_{exp}(q)$, was computed as:

$$S_{exp}(q) = \frac{I(q) - \left(< f^2 > - < f >^2\right)}{< f >^2}$$

where: $I(q)$ is the coherently scattered intensity, normalized to electron units, $< f^2 > = \sum_{i=1}^{n} c_i f_i^2$, $< f > = \sum_{i=1}^{n} c_i f_i$, c_i and f_i are the concentration and the atomic scattering factor of the i-th atomic species, respectively, and n is the number of atomic species in the sample. The Q-function of scattering intensity for the separate PMMS in nanopores was derived from a

difference between the normalized scattering intensity for the confined system and the empty porous matrix[6].

NUMERICAL MODELLING SECTION

Model and simulation methodology. Molecular dynamics simulations of oligomers in a bulk and in a cylindrical nanopore were performed at coarse-grained resolution using bead-spring model where monomers were represented by spheres. In our simulations, the backbone of an oligomer was composed of $N_b = 10$ beads. To mimic architecture of PMMS and PMPS side chains, each backbone monomer was also connected to a single side bead, i.e., $N_s = 1$. The total number of beads in an oligomer molecule was $N = N_b + N_b N_s = 20$. The non-bonded interactions between beads, separated by a distance r, were modeled by the truncated and shifted Lennard-Jones (LJ) potential

$$V^{LJ}(r) = \begin{cases} 4\epsilon\left[(\sigma/r)^{12} - (\sigma/r)^6 + \left(\sigma/r_c\right)^{12} - \left(\sigma/r_c\right)^6\right] & r \le r_{cut} \\ 0 & r > r_{cut,} \end{cases} \quad \text{(Eq. 1)}$$

where ϵ and σ are respectively the units of energy and length and r_{cut} is the potential cutoff distance. We take $\sigma = 1$ and $\epsilon = 1$. The latter is in units of thermal energy kT with k being the Boltzmann's constant. The bead-bead interactions were modeled via a purely repulsive LJ potential with a cutoff $r_{cut} = 2^{1/6}\sigma$. The bonded interactions in an oligomer were mimicked by the Kremer-Grest potential,[7,8] 1,2 $V^{KG}(r) = V^{FENE}(r) + V^{LJ}(r)$, with the "finite extensible nonlinear elastic" (FENE) potential

$$V^{FENE} = -\frac{1}{2}k_F r_F^2 \, ln\left[1 - \left(r/r_F\right)^2\right]. \quad \text{(Eq. 2)}$$

In (Eq. 2) the bond spring-constant is $k_F = 30\epsilon/\sigma^2$, and the maximum bond length is $r_F = 1.5\sigma$. In our experiments we utilized polymers with low molecular weights, i.e., with contour length smaller than their persistence length. Consequently, individual oligomeric molecules are expected to be rather stiff. In simulations the stiffness of oligomeric chains was introduced by a bond-bending potential which acts on three consecutive backbone beads. The bending potential reads

$$V^B = k_B[1 - \cos(\theta_{ijk})], \quad \text{(Eq. 3)}$$

In the equation above, k_B is bending stiffness and θ_{ijk} is the angle between the two subsequent backbone bond vectors $\vec{b}_i \equiv \vec{r}_{i+1} - \vec{r}_i$ and $\vec{b}_{i+1}$, where vectors $\vec{r}_{i+1}$ and $\vec{r}_i$ denote positions of two consecutive backbone beads.

In simulations, we also constrained planarity of molecules via four-bead torsional potential

$$V^T = k_T[1 + \cos(\varphi_{ijkl})]. \qquad \text{(Eq. 4)}$$

In (Eq.4) k_T is torsional stiffness and φ_{ijkl} is the dihedral angle which is defined between three consecutive bond vectors $\vec{b}_{i-2}$, $\vec{b}_{i-1}$ and $\vec{b}_i$ connecting side-backbone, backbone-backbone and backbone-side beads, respectively. We carried out simulations for three molecular models of oligomers with different bending and torsional interactions. We denoted these models, as model I, II and III. In model I oligomers have flexible backbones and side beads. In model II we consider stiff backbones and flexible side beads, whereas in model III incorporates stiff backbones and planar side beads. The latter feature in model III is due to torsional interactions. Table 1 summarizes all parameters incorporated in all models that were utilized in our study.

Model	k_B/ϵ	k_T/ϵ
I	0	0
II	100	0
III	100	10

Table 1. Summary of model parameters used for coarse-grained molecular simulations of oligomers. k_B and k_T are bending and torsional stiffness from (Eqs. 3) and (4), respectively.

Newton's equations of motion were solved using a velocity Verlet algorithm. A Langevin damping term with damping $\zeta = 0.5m\tau^{-1}$ was used, where $\tau = \sqrt{m\sigma^2/\epsilon}$ is the LJ time unit and $m = 1$ is the bead mass. The integration step was taken to be $\Delta\tau = 0.002\tau$, and the thermal energy was constant at $k_BT = \epsilon$. All simulations were carried out using the Large-scale Atomic/Molecular Massively Parallel Simulator (LAMMPS),[9] and simulation snapshots were rendered using the program Visual Molecular Dynamics (VMD).[10]

Simulations in a bulk were performed in a cubic box of length L at melt number density $0.85\sigma^{-3}$. We imposed periodic boundary conditions in all spatial dimensions. All systems contained $M = 3500$ oligomers. As a starting configuration, we used oligomers placed randomly in a simulation cell. Oligomers were generated using a self-avoiding random walk

technique. The initial density for all systems was low $\approx 10^{-4}\sigma^{-3}$. To obtain the bulk density, the simulation box was gradually decreased in size at constant velocity $10^{-3}\sigma\tau^{-1}$. Once the target density was reached, simulations were continued in order to obtain equilibrium bulk morphology. This final part of simulation was running for at least three relaxation times τ_R of the corresponding system, where τ_R is defined as the relaxation time of the backbone end-to-end distance autocorrelation function.

The cylindrical pore was modeled as structureless, impenetrable and repulsive rigid wall. We assume bead-wall interactions of the same form as in (Eq. 1). The only differences are choosing cylindrical coordinates and replacing r by $D/2-r$ in (Eq. 1), where D is cylinder diameter. These simulations were conducted for $M = 2400$ oligomeric chains. We applied periodic boundary conditions along the cylinder axis. Initially chains were distributed randomly inside a cylindrical volume with large diameter and height corresponding to low density $5{\cdot}10^{-3}\sigma^{-3}$. Subsequently, the diameter of the pore was gradually decreased to the effective value $D_0 = D - 2^{1/6}\sigma$. This reduction in diameter size is due to wall depletion which restricts the space available for confined oligomers. In the following step, the cylinder height was adjusted to achieve the final density $0.85\sigma^{-3}$, the same as in the bulk simulations. Finally, simulation was followed by a production run lasting $10^6\tau$.

By taking time and ensemble averages over equilibrium configurations, denoted here symbolically as $\langle\cdots\rangle$, several quantities of interest were sampled. Similarly, to our experiments, the internal structure of melts was analyzed using the static structure factor which reads[11]

$$S(q) = \sum_{i=1}^{NM}\sum_{j=1}^{NM}\left\langle e^{-i\vec{q}\cdot(\vec{r_i}-\vec{r_j})}\right\rangle . \qquad \text{(Eq. 5)}$$

References

(1) Tarnacka, M.; Jurkiewicz, K.; Hachuła, B.; Wojnarowska, Z.; Wrzalik, R.; Bielas, R.; Talik, A.; Maksym, P.; Kaminski, K.; Paluch, M. Correlation between Locally Ordered (Hydrogen-Bonded) Nanodomains and Puzzling Dynamics of Polymethysiloxane Derivative. *Macromolecules* **2020**, *53* (22), 10225–10233. https://doi.org/10.1021/acs.macromol.0c01289.

(2) Tu, W.; Ngai, K. L.; Paluch, M.; Adrjanowicz, K. Dielectric Study on the Well-Resolved Sub-Rouse and JG β-Relaxations of Poly(Methylphenylsiloxane) at Ambient and Elevated Pressures. *Macromolecules* **2020**, *53* (5), 1706–1715. https://doi.org/10.1021/acs.macromol.9b02332.

(3) Iacob, C.; Sangoro, J. R.; Papadopoulos, P.; Schubert, T.; Naumov, S.; Valiullin, R.; Kärger, J.; Kremer, F. Charge Transport and Diffusion of Ionic Liquids in Nanoporous Silica Membranes. *Phys. Chem. Chem. Phys.* **2010**, *12* (41), 13798. https://doi.org/10.1039/c004546b.

(4) Kipnusu, W. K.; Kossack, W.; Iacob, C.; Jasiurkowska, M.; Rume Sangoro, J.; Kremer, F. Molecular Order and Dynamics of Tris(2-Ethylhexyl)Phosphate Confined in Uni-Directional Nanopores. *Zeitschrift für Phys. Chemie* **2012**, *226* (7–8), 797–805. https://doi.org/10.1524/zpch.2012.0287.

(5) Talik, A.; Tarnacka, M.; Geppert-Rybczyńska, M.; Hachuła, B.; Bernat, R.; Chrzanowska, A.; Kaminski, K.; Paluch, M. Are Hydrogen Supramolecular Structures Being Suppressed upon Nanoscale Confinement? The Case of Monohydroxy Alcohols. *J. Colloid Interface Sci.* **2020**, *576*, 217–229. https://doi.org/10.1016/j.jcis.2020.04.084.

(6) Morineau, D.; Alba-Simionesco, C. Liquids in Confined Geometry: How to Connect Changes in the Structure Factor to Modifications of Local Order. *J. Chem. Phys.* **2003**, *118* (20), 9389–9400. https://doi.org/10.1063/1.1568932.

(7) Kremer, K.; Grest, G. S. Dynamics of Entangled Linear Polymer Melts: A Molecular-Dynamics Simulation. *J. Chem. Phys.* **1990**, *92* (8), 5057–5086. https://doi.org/10.1063/1.458541.

(8) Grest, G. S.; Kremer, K. Molecular Dynamics Simulation for Polymers in the Presence of a Heat Bath. *Phys. Rev. A* **1986**, *33* (5), 3628–3631. https://doi.org/10.1103/PhysRevA.33.3628.

(9) Plimpton, S. Fast Parallel Algorithms for Short-Range Molecular Dynamics. *J. Comput. Phys.* **1995**, *117* (1), 1–19. https://doi.org/10.1006/jcph.1995.1039.

(10) Humphrey, W.; Dalke, A.; Schulten, K. VMD: Visual Molecular Dynamics. *J. Mol. Graph.* **1996**, *14* (1), 33–38. https://doi.org/10.1016/0263-7855(96)00018-5.

(11) Julia S. Higgins and Henri C. Benoit. *Polymers and Neutron Scattering*; Clarendon Press, 1997.